Chemical Engineering Journal 527 (2026) 171875

Contents lists available at ScienceDirect

Chemical Engineering Journal

journal homepage: www.elsevier.com/locate/cej

Zwitterion-functionalized gel electrolyte via anion-cation regulation enables rapid Zn^{2+} kinetics for low-temperature zinc batteries

Mengfan Zhao [a,1], Xueqing Chen [a,1], Shuai Liu [a], Rujian Fu [a], Bao Li [a], Lifeng Hou [a,*], Shi Wang [b,d,*], Zhong Jin [c,*], Qian Wang [a,*]

[a] College of Materials Science and Engineering, Taiyuan University of Technology, Taiyuan, 030024, Shanxi, China
[b] State Key Laboratory of Flexible Electronics (LoFE) & Institute of Advanced Materials (IAM), Nanjing University of Posts & Telecommunications, 9 Wenyuan Road, Nanjing 210023, China
[c] State Key Laboratory of Coordination Chemistry, MOE Key Laboratory of Mesoscopic Chemistry, MOE Key Laboratory of High Performance Polymer Materials and Technology, Jiangsu Key Laboratory of Advanced Organic Materials, Suzhou Key Laboratory of Green Intelligent Manufacturing of New Energy Materials and Devices, Tianchang New Materials and Energy Technology Research Center, Institute of Green Chemistry and Engineering, School of Chemistry and Chemical Engineering, Nanjing University, Nanjing, 210023, China
[d] Key Laboratory of Functional Molecular Solids, Ministry of Education, Anhui EngineeringResearch Center of Carbon Neutrality, College of Chemistry and Materials Science, Anhui Normal University, Wuhu 241000, China

ARTICLE INFO

Keywords:
Zn metal anode
Zinc batteries
Gel electrolyte
Interface
Zwitterion

ABSTRACT

Gel electrolytes have shown great promise for rechargeable Zn-ion batteries due to their high safety and excellent plasticity. However, they still face serious challenges at low temperatures, such as: electrolyte freezing and a dramatic rise in charge transfer resistance, leading to huge kinetic barriers and unstable electrode-electrolyte interface, greatly hindering their practical application. Herein, this work propose a synergistic molecular engineering strategy by introducing a polyzwitterion (poly(3-[(3-Acrylamidopropyl)dimethylammonio]propane-1-sulfonate) into the polyacrylamide (PAM)-based hydrogel framework to construct a dynamic, multi-crosslinked and zwitterionic-functionalized gel electrolyte system. Among them, the effective dynamic crosslinking between polyzwitterion and PAM segments not only significantly improves the stretchability of gel electrolyte (with a strain of 1200 %), but also widens the spacing between polymer chains. Together with its intrinsic anion–cation interactions of polyzwitterion segments, a continuous and high-speed ion channel is formed, enabling rapid and stable Zn^{2+} transport. Simultaneously, polyzwitterion segments can also immobilize anions from Zn salt and bound active H_2O molecules via its charged groups, lowering the freezing point of the electrolyte to below −40 °C and improving the Zn^{2+} transference number (0.92), surpassing those of most state-of-the-art gel electrolytes (<0.75), thereby achieving a robust SEI layer with a thickness of only ~11 nm. Consequently, the optimized gel electrolyte demonstrates a high ionic conductivity of 13.54 mS cm^{-1} and rapid Zn^{2+} kinetics. When paired with I_2, NVO and PANI cathodes, all the full cells deliver high specific capacities and long cycling life even at −40 °C. This work offers a feasible zwitterionic-functionalized strategy for designing high-performance gel electrolytes toward low-temperature application.

1. Introduction

Aqueous zinc-ion batteries (AZIBs) have garnered widespread research interest due to their high theoretical capacity, low redox potential, high safety, and cost-effectiveness [1]. Nevertheless, in a conventional aqueous electrolyte, Zn metal anode often faces severe dendrite growth and parasitic side reactions (e.g. hydrogen evolution reaction, surface corrosion), leading to poor coulombic efficiency and short cycling life, severely hindering the practical application of AZIBs [2,3].

In recent years, hydrogel electrolytes have been proposed as an effective alternative because they can suppress dendritic Zn growth through high mechanical strength and disrupt the hydrogen bond network between H_2O molecules, minimizing H_2O activity and reducing

* Corresponding authors.
E-mail addresses: houlifeng@tyut.edu.cn (L. Hou), iamshiwang@njupt.edu.cn (S. Wang), zhongjin@nju.edu.cn (Z. Jin), qianwang0825@pku.edu.cn (Q. Wang).
[1] The authors contributed equally to this work.

https://doi.org/10.1016/j.cej.2025.171875
Received 27 October 2025; Received in revised form 2 December 2025; Accepted 12 December 2025
Available online 13 December 2025

interface side reactions [4,5]. Moreover, their flexibility and adhesion facilitate the stable electrode-electrolyte contact, promoting homogeneous Zn^{2+} ion flux. However, conventional hydrogel electrolytes exhibit severe limitations at low temperature, especially below −20 °C [6]. The freezing of the aqueous phase and increased charge-transfer resistance, as well as loss of viscoelasticity under low temperature conditions collectively result in slow ion transport, severe polarization and even mechanical failure, rendering them impractical for low-temperature applications [7].

In the past decades, several strategies have been explored to improve the low-temperature performance of hydrogel electrolytes, including designing new hydrogel electrolyte materials, introducing organic co-solvents or concentrated salts, engineering nano-porous structures, developing organic–inorganic composite systems [8]. These approaches primarily aim to regulate the hydrogen bonding network within the electrolyte and optimize the Zn^{2+} transport pathways, thereby improving Zn^{2+} transport kinetics at low temperature. Unfortunately, these strategies will more or less affect the interfacial compatibility [9]. E.g.: while nano-porous structures facilitate ion movement, they offer limited control over the formation of the SEI layer [10]. Deep eutectic salt systems or concentrated salts will inevitably promote the formation of insulating by-products, such as: $Zn_5(OH)_8Cl_2{\cdot}H_2O$, leading to thick and highly resistive SEI layer [11,12]. Organic–inorganic hybrids (e.g., SiO_2-enhanced gels) suffer from severe brittleness at low temperature due to polymer chain freezing and mismatched thermal expansion, resulting in poor interface contact and repetitive cracking. However, their $t_(Zn^{2+})$ values are still below 0.8, limiting the ultimate kinetics and reversibility [13–15]. Parallel to this, the formation of a thin and robust SEI is equally critical yet challenging. Recent strategies have reported SEI layers with thicknesses ranging from >100 nm [16–18]. More critically, these issues often interplay synergistically, further aggravating performance degradation. As a result, developing innovative strategies to break the inherent hydrogen bond network and construct fast Zn^{2+} transport channels, while promoting the formation of thin and robust SEI film to enhance Zn^{2+} kinetics and tolerance to low temperature, holds significant promise for realizing the practical application of AZIBs [19].

Herein, a molecularly engineered zwitterion-functionalized gel electrolyte specifically designed for low-temperature application is developed. The electrolyte is constructed by incorporating glycine (Gly) and the polyzwitterion poly(3-[(3-Acrylamidopropyl) dimethylammonio]propane-1-sulfonate (PDAPS) into a PAM-based hydrogel electrolyte, forming a copolymer with a dynamic multi-crosslinked structure [20]. In this system, PAM serves as a mechanical backbone, Gly enhances hydrophilicity and strengthens hydrogen bonding, while PDAPS—grafted as side chains with oppositely charged groups—acts as a dynamic modulator. The polyzwitterion reorganizes free water molecules and inhibits ice crystallization, depressing the freezing point of the electrolyte to below −40 °C. Moreover, the copolymerization of PDAPS expands the interchain spacing within the polymer network, together with its intrinsic anion–cation interactions, forming continuous ion-conducting channels that yield high ionic conductivity of 13.54 mS cm^{-1} at room temperature. During electrochemical cycling, PDAPS segments can also immobilize anions from Zn salt via its charged groups, increasing the Zn^{2+} transference number to 0.92, thereby promoting the formation of a uniform and robust SEI layer with a thickness of only ~11 nm, which significantly reduces interfacial resistance and promotes highly reversible Zn plating/stripping. As a result, the full cells employing this gel electrolyte with I_2, NVO and PANI cathodes exhibit high specific capacity and prolonged cycling stability, even at −40 °C, demonstrating great potential for practical application of AZIBs.

2. Results and discussion

2.1. Design concept and electrolyte structure

For a typical gel electrolyte in AZIBs, its main role is to maintain the inherent safety, while maximizing the free water confinement, broadening the electrochemical stability window and suppressing side reactions [21,22]. To this end, hydrophilic group-rich polymers are typically employed to immobilize H_2O molecules onto polymer frameworks via hydrogen bonding or electrostatic interactions, thereby reducing H_2O activity and improving electrochemical stability [23]. Acrylamide is widely regarded as an ideal backbone-forming monomer due to its excellent H_2O solubility and high polymerization efficiency [24]. However, the mechanical robustness and ionic conductivity of a PAM network remain inadequate [25,26]. To address this, Gly was incorporated into the PAM-based hydrogel framework to form high-density hydrogen bonding cross-links with the PAM network and immobilize water molecules, thus reducing the amount of free water and improving mechanical strength. As shown in Fig. S1, after introducing Gly into the PAM-based hydrogel, the contact angle had decreased from 75.9° to 59.6°, indicating improved hydrophilicity, which can be attributed to the abundance of O—H bonds in Gly [27]. Then, the zwitterion of DAPS was introduced into this system to form a copolymer, further enhancing water confinement and ion transport behavior. The numerous hydrophilic and charged groups of DAPS can effectively immobilize water molecules, mitigating HER. Simultaneously, the carbonyl groups of DAPS can form a dense hydrogen-bonding network with PAM and Gly, weaving initially loose polymer segments into a compact and homogeneous multi-crosslinked framework, thereby significantly improving mechanical strength and structural stability. In addition, the zwitterionic side chains of DAPS electrostatically “expand” the polymer molecular chains, creating high-speed Zn^{2+} transport channels. As shown in Fig. 1, the zwitterionic-functionalized gel electrolyte can remain highly flexible and rapid Zn^{2+} kinetics even at −40 °C. Moreover, DAPS can also immobilize anions from Zn salt via its charged groups, improving the Zn^{2+} transference number, thereby promoting the formation of a uniform and robust SEI layer.

According to the latest reports, the state of water molecules within gel electrolytes, dictated by their hydrogen bond strength, is a critical factor governing ionic conductivity and interfacial stability [28]. Thus, this work conducted spectroscopic analyses focused on hydrogen-bond evolution. As shown in Figs. 2a and S2, compared to the pure PAM hydrogel electrolyte; after introducing DAPS, the O—H band broadened significantly in the zwitterion-functionalized gel electrolyte, indicating a restructuring of the hydrogen-bonding environment [29,30]. Furthermore, this work also conducted hydrogen bond analysis using Raman spectroscopy and decomposed the O—H vibration into three types of hydrogen bonds through Gaussian fitting As shown in Fig. 2b & c, for the pure PAM hydrogel electrolyte, medium hydrogen (MH) bonds predominated, with strong hydrogen (SH) bonds and weak hydrogen (WH) bonds accounting for 17.1 % and 20.2 %, respectively. And the introduction of Gly provided dual hydrogen donor/acceptor sites via its –COOH and $–NH_2$ groups, forming an additional Gly–H_2O hydrogen-bonding network that reduced the proportion of SH bonds to ~12 %. With further incorporation of DAPS, the $–SO_3^-$ groups and quaternary ammonium groups can further bind with water molecules, markedly disrupting the original network water structure [31]. Thus, the proportion of SH bonds plummeted to 8.7 %, while WH bonds surged to 33.8 %. This transition from SH bonds to WH bonds significantly reduced the average binding energy of water molecules, lowering the freezing point of the gel electrolyte.

Then, DFT calculations were employed to analyze the Zn^{2+} coordination environment and the binding energy between electrolyte and water molecules [32]. As shown in Fig. 2d, DAPS exhibited the highest binding energy with water molecules, offering a molecular explanation for the sharp decrease in freezing point. Subsequently, differential

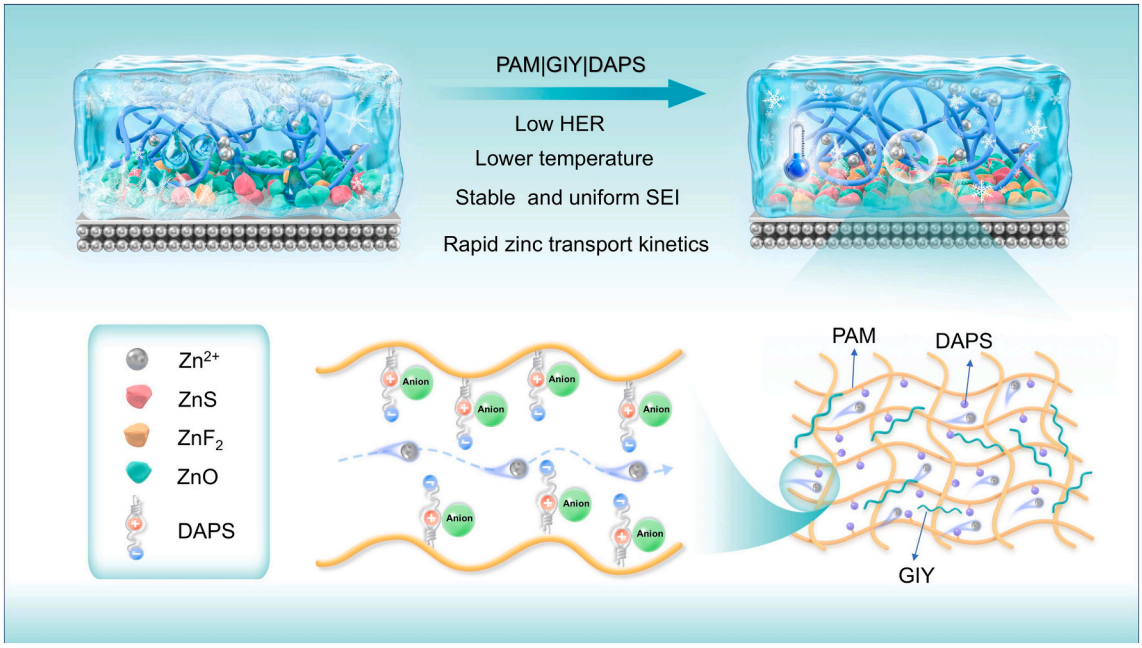

Fig. 1. Schematic diagram of zinc ion deposition and transportation in zwitterion-functionalized gel electrolyte.

scanning calorimetry (DSC) measurements revealed that the incorporation of DAPS leaded to a dramatic suppression of freezing, causing the electrolyte freezing point to drop to −42.7 °C, enabling the battery to operate stably under low temperature conditions (Fig. 2e). Furthermore, DAPS also showed the highest binding energy with $CF_3SO_3^-$ (anions from Zn salt), helping to increase the Zn^{2+} transference number, attributable to the strong electrostatic effects of its quaternary ammonium cations (Fig. 2f). Meanwhile, the Zn^{2+} coordination environment was analyzed by means of the radial distribution function (RDF). As shown in Fig. 2g-i, after introducing the Gly into the pure PAM hydrogel electrolyte, the average coordination number for Zn^{2+} with H_2O decreased from 4.96 to 4.72, suggesting Gly can form hydrogen bonds with H_2O molecules, thereby weakening the interaction between Zn^{2+} and H_2O. And after introducing the zwitterion of DAPS into the PAM to form a copolymer, the average coordination number for Zn^{2+} with H_2O decreased again, indicating that DMPS can further lock water and reduce side reactions, such as: HER. Meanwhile, the zwitterionic-functionalized gel electrolyte exhibited weak Zn–O(DAPS) coordination alongside enhanced Zn–O (Gly) coordination, indirectly evidencing DAPS-induced expansion of the inter-chain spacing and the resultant engagement of additional free Gly molecules in Zn^{2+} coordination.

^1H NMR chemical shifts further support these trends. As shown in Fig. S3, ^1H NMR spectra of $Zn(OTF)_2$ recorded after the addition of PAM, GIY or DAPS reveal an obvious up-field shift and simultaneous narrowing of the water ^1H signal [33]. This behavior is ascribed to the zwitterionic DAPS: its paired positive and negative centers anchor framework anions through a combination of electrostatic and hydrogen-bonding interactions, enriching the local electron density around water and increasing its shielding. Concurrently, DAPS lowers the energy barrier for water exchange, accelerating the rate so that the system approaches the fast-exchange limit, which manifests as a sharper peak. ^{19}F NMR also demonstrated the change of coordination environment. As shown in Fig. 2j compared to pure PAM hydrogel electrolyte, the ^{19}F peak in the NMR spectra resonance exhibits a clear upfield shift after introducing the Gly, suggesting an increase in the electron density because of $CF_3SO_3^-$ detachment from the solvated sheath. And after introducing the DAPS into the PAM to form a copolymer, because the zwitterionic side chains of DAPS electrostatically “expand” the polymer molecular chains, more Gly and $CF_3SO_3^-$ participated in coordination, the ^{19}F peak in the NMR spectra exhibited a slight up-field shift. Electronic structure calculations further revealed that DAPS had a higher HOMO energy level than PAM and Gly, suggesting that it was easy to decompose and form a ZnS-rich SEI film during electrochemical cycles (Fig. 2k) [34,35].

To sum up, the copolymerization of DAPS can significantly lower the freezing point of gel electrolytes and expand the interchain spacing within the polymer network through its intrinsic anion–cation interactions, enabling rapid and stable Zn^{2+} transport at low temperature. Meanwhile, its high HOMO energy level and strong interaction with anions from Zn salt can induce the formation of a uniform and robust SEI layer enriched with ZnS and ZnF_2, improving interface stability.

2.2. Gel electrolyte properties and Zn^{2+} diffusion

To systematically assess the influence of DAPS on the intrinsic properties of the gel electrolyte, this work performed thermogravimetric (TG) analysis, tensile tests, and electrochemical tests. As shown in Fig. 3a, compared to the pure PAM hydrogel electrolyte, with the copolymerization of DAPS, the zwitterionic-functionalized gel electrolyte displayed a higher thermal stability and lower weight loss, highlighting its excellent water locking ability [36]. Mechanical characterization revealed that the elongation at break of the pure PAM hydrogel was 449 % (Fig. 3b). With the incorporation of Gly, additional hydrogen bonding via –COOH groups increased this value to 660 %. Further copolymerization of DAPS leaded to the formation of a dynamic and multi-crosslinked network, where synergistic hydrogen bonding and electrostatic interactions raised the elongation at break dramatically to 1265 %, demonstrating exceptional tensile toughness [37]. For the electrochemical stability, linear sweep voltammetry (LSV) demonstrated that the electrochemical window of hydrogel electrolyte was expanded to >2.5 V after introducing the DAPS, which can match with common cathode materials (Fig. 3c).

The Zn^{2+} diffusion is directly governed by the ionic conductivity of gel electrolytes, which can be quantified by electrochemical impedance spectroscopy (EIS). As shown in Fig. 3d, the pure PAM gel electrolyte exhibited a conductivity of 8.45 mS cm^{-1}. However, with the copolymerization of DAPS, the ionic conductivity of the zwitterionic-functionalized gel electrolyte had increased to 13.54 mS cm^{-1}, which

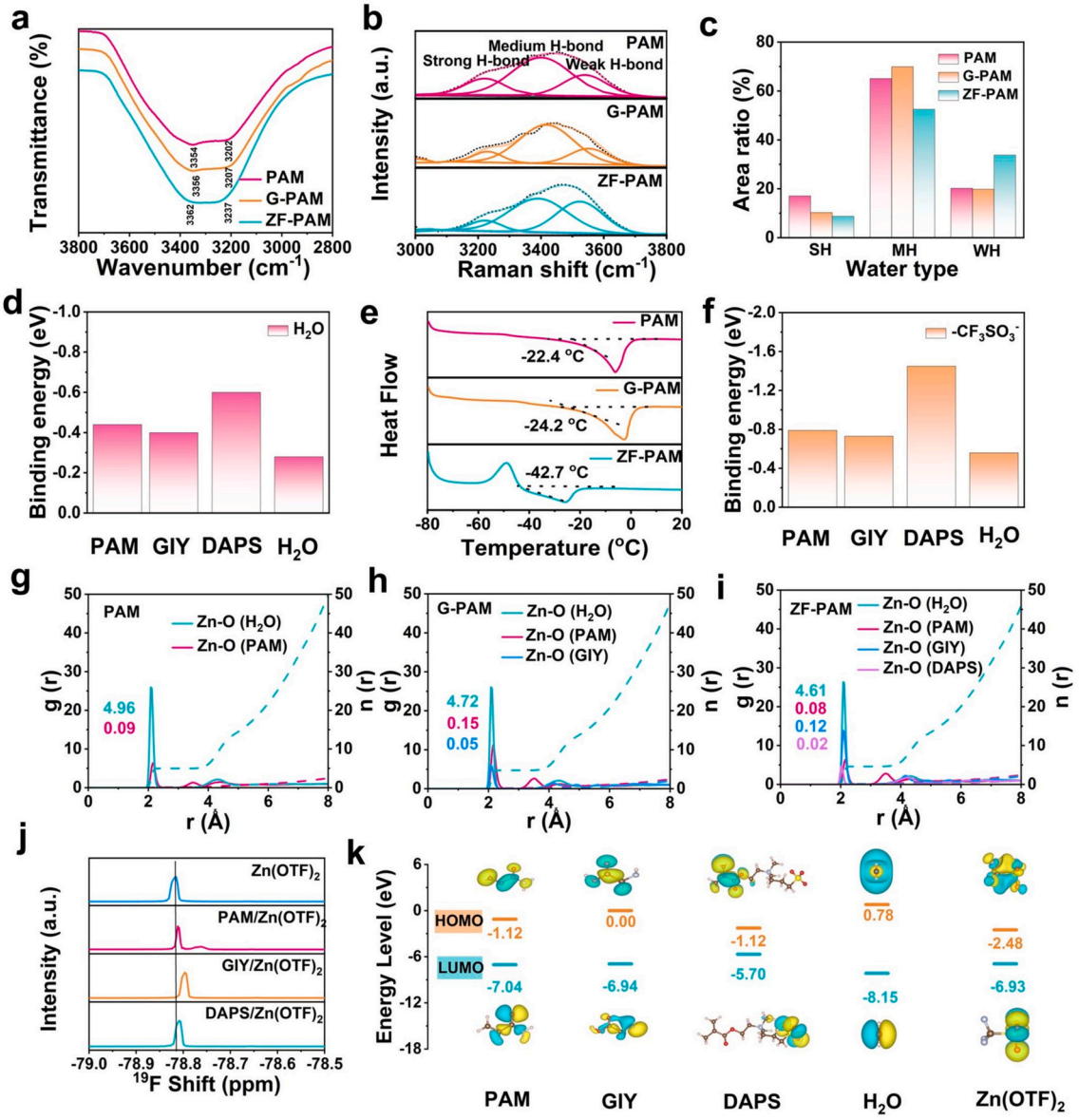

Fig. 2. Solvation structure and Zn^{2+} diffusion mechanism. a) FT-IR spectra; b) fitting Raman spectra of O—H stretching vibrations; c) different types of water in the gel electrolyte; d) binding energies with H_2O; e) DSC curves; f) binding energies with $CF_3SO_3^-$; g-i) radial distribution function and coordination number of Zn—O in the gel electrolyte; j) ^{17}F nuclear magnetic resonance (NMR) spectrum; k) HOMO and LUMO energy levels.

can be attributed to the high-speed Zn^{2+} transport channels created by the anion–cation interaction of zwitterionic DAPS side chains. To further evaluate the practical applicability of the PDAPS-based gel electrolyte under low-temperature conditions, we measured its ionic conductivity from 25 °C to −40 °C. As shown in Figs. S4 & S5, the electrolyte maintained a high conductivity of 6.18 mS cm^{-1} even at −40 °C, demonstrating remarkably retained ion-transport capability in low-temperature environments. Beyond bulk ionic conductivity, the Zn^{2+} transference number also critically reflected the contribution of cations to charge transport. As shown in Figs. 3e & f and S6, the Zn^{2+} transference number of the zwitterionic-functionalized gel electrolyte was as high as 0.92, which was much higher than that of the pure PAM gel electrolyte (0.43) and the PAM-based gel electrolyte with Gly addition (0.56). This high Zn^{2+} transference number close to a single ion channel was essential for high-rate and long-life batteries. This once again indirectly proved that DAPS can also immobilize anions from Zn salt and widen the spacing between polymer chains. Furthermore, mean square displacement (MSD) analysis further confirmed the enhanced Zn^{2+} diffusivity. As shown in Fig. 3g, the zwitterionic-functionalized gel electrolyte incorporating DAPS demonstrated a higher Zn^{2+} diffusion coefficient compared to the pure PAM gel electrolyte, which can be attributed to the high-speed Zn^{2+} transport pathways established through the anion–cation interaction of the zwitterionic side chains in DAPS.

After that, this work performed EIS on symmetric cells at various temperatures and derived the de-solvation activation energy (E_a). As shown in Figs. 3h and S7, compared with the pure PAM gel electrolyte, the zwitterionic-functionalized gel electrolyte incorporating DAPS demonstrated a smaller de-solvation energy (E_a = 22 kJ mol^{-1}), indicating that the Zn^{2+} migration barrier at the electrode/electrolyte interface was greatly weakened, enabling rapid and reversible Zn deposition even at low temperature. The cyclic voltammetry curves of Zn | Cu half cells further supported this conclusion, which is associated with promoting the formation of large nuclei, resulting in fine-grained dense zinc deposition. (Figs. 3i and S8) [38]. This lowered de-solvation energy is attributed to the significant modification of the

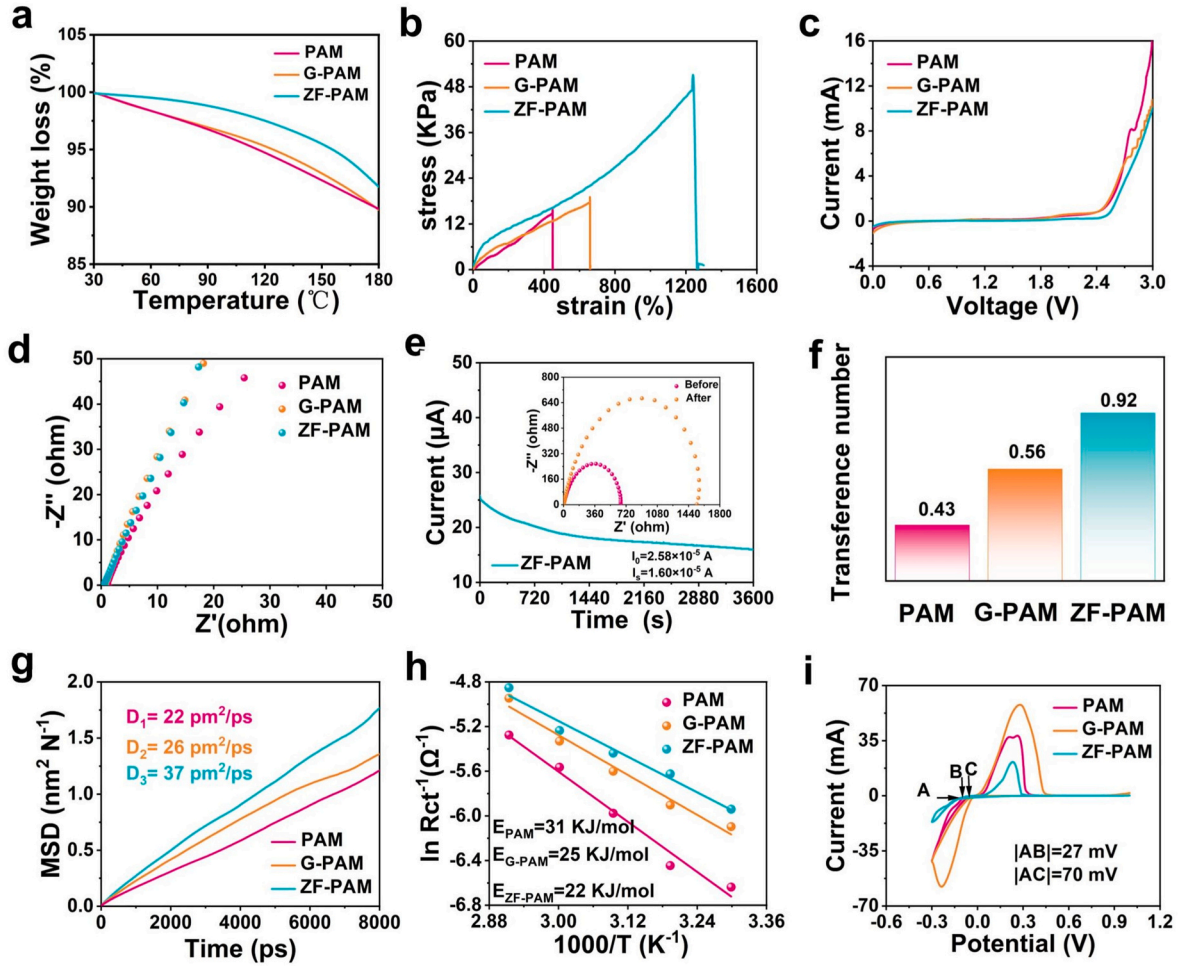

Fig. 3. Characterization of gel electrolyte properties and Zn^{2+} diffusion. a) Thermogravimetric analysis (TG) curves; b) stress-strain curves; c) LSV of the gel electrolytes; d) EIS spectra of SS || SS cells of the gel electrolytes; e) Zn^{2+} transference number of the gel electrolyte; f) Zn^{2+} transfer number of different gel electrolytes; g) simulations of the Zn^{2+} diffusion coefficient in the gel electrolyte via MSD analysis; h) activation energy; i) CV curve of Cu—Zn battery.

Zn^{2+} solvation structure induced by the zwitterionic network. The increased proportion of weakly-bound water molecules and the reduced coordination number of Zn^{2+} with H_2O collectively weaken the Zn^{2+}-H_2O interactions, thereby facilitating easier de-solvation at the interface.

2.3. *Interface behavior analysis and SEI film*

The charge storage in this work follows a hybrid mechanism resulting from the synergy between fast interfacial kinetics and bulk diffusion. The high Zn^{2+} transference number (0.92) and the low de-solvation energy (22 kJ mol^{-1}) enabled by the PDAPS electrolyte significantly enhance the interfacial charge transfer kinetics. Simultaneously, the continuous ion channels formed by the electrolyte, together with the stable SEI layer on the anode side, ensure effective Zn^{2+} transport. To explore the advancement of such a zwitterionic-functionalized gel electrolyte in stabilizing interface, this work first evaluated the self-corrosion behavior. As shown in Fig. 4a, Tafel polarization measurements revealed a positive shift in corrosion potential from −26 mV to 44 mV after introducing the DAPS, along with an order-of-magnitude reduction in corrosion current density, indicating effective H_2O immobilization and improved interface stability [39]. According to previous reports, the self-corrosion behavior and the hydrogen evolution reaction occur simultaneously. Subsequently, this work analyzed the hydrogen evolution potential of the zwitterionic-functionalized gel electrolyte systems, which was shown in Fig. 4b. Introducing DAPS into the gel electrolyte shifted the hydrogen-evolution overpotential markedly to more negative values, indicating a suppressed hydrogen-evolution reaction.

Furthermore, this work also explores the interface stability during the electrochemical deposition process by in-situ impedance and corresponding DRT analysis [40]. As shown in Figs. 4c-e and S9, in-situ impedance monitoring demonstrated that the zwitterionic-functionalized gel electrolyte exhibited minimal impedance fluctuation throughout Zn deposition process, with nearly overlapping Nyquist curves. In contrast, the impedance arc of the pure PAM gel electrolyte system and the gel electrolyte only with Gly addition continued to expand, indicating progressive interfacial degradation. Further distribution of relaxation times (DRT) analysis of the EIS data confirmed outstanding interfacial stability for the zwitterionic-functionalized gel electrolyte system: the position and intensity of relaxation peaks remained almost unchanged through the whole testing process, significantly outperforming the control group, once again demonstrating the positive role of the copolymerization of DAPS in improving interface stability. Correspondingly, the Zn nucleation and deposition behavior was also investigated by chronoamperometry curves. As shown in Fig. 4f, the response current in the pure PAM gel electrolyte increased continuously, suggesting a constant two-dimensional diffusion mechanism, thus lowering interfacial stability and resulting in irregular 3D Zn deposition structure. In contrast, after adding Gly, a clear nucleation platform appeared in the chronoamperometry curves, corresponding to a stable three-dimensional diffusion, and subsequent copolymerization of DAPS further sustained this three-dimensional diffusion behavior.

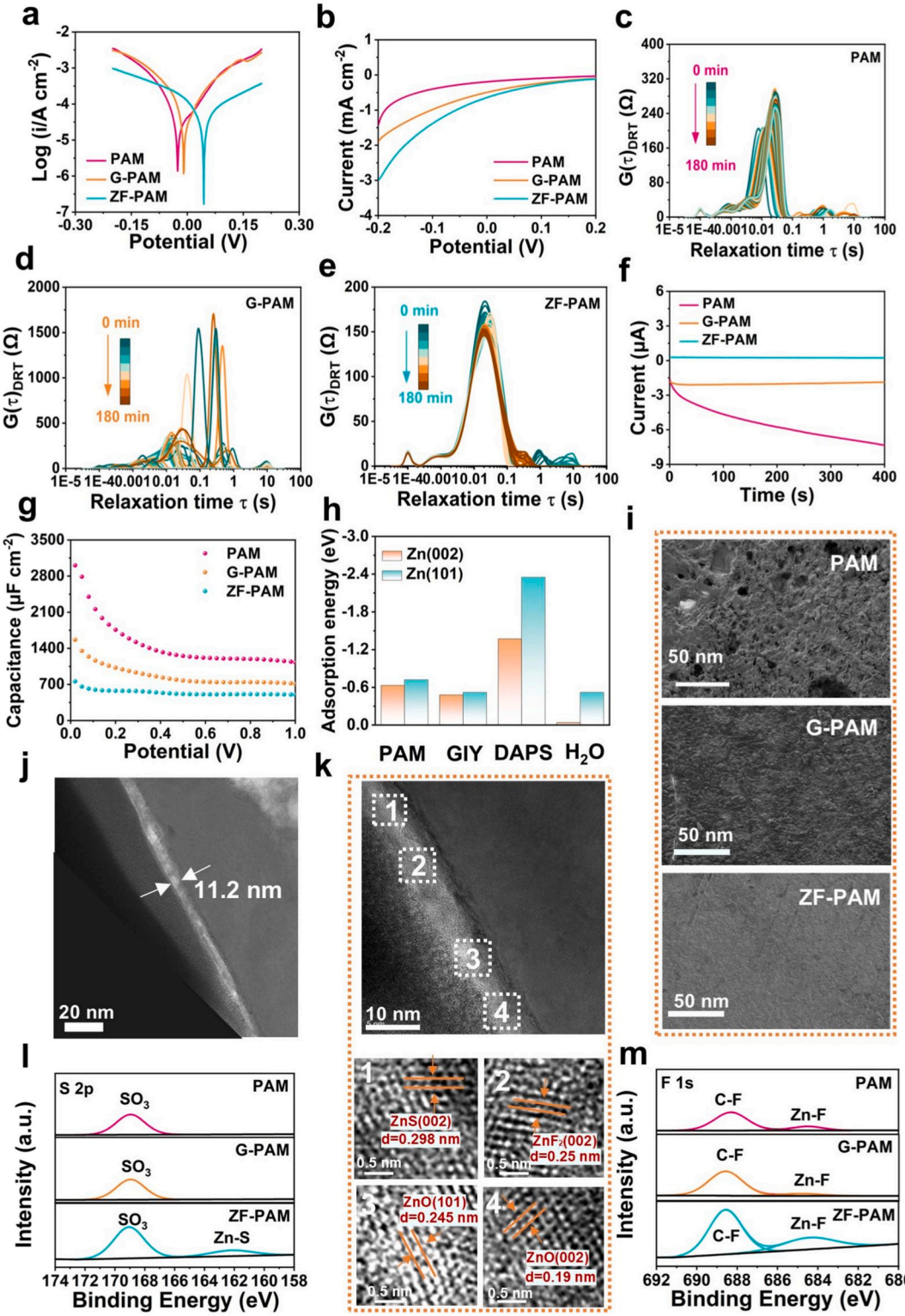

Fig. 4. Corrosion and interface behavior analysis. a) Tafel curve; b) hydrogen evolution overpotential; c & e) DRT analysis of Zn||Zn cells; f) chronoamperograms at an overpotential of −150 mV; g) the non-Faradaic capacitance-potential curve; h) adsorption energy on different crystal planes; i) SEM images of Zn metal anode after 50 cycles in the gel electrolytes; j & k) HRTEM image of SEI film formed in the gel electrolyte; l & m) XPS spectra of Zn metal anode after 50 cycles, S 2p (l); F 1s (m).

The enhanced diffusion not only effectively dissipated interfacial ion concentration gradients but also promoted the lateral and parallel Zn deposition, enabling high interfacial stability and dendrite-free Zn surface.

At the same time, AC-voltammetry-derived differential capacitance profiles reveal that pure PAM gel electrolyte with its loose network and abundant polar groups, builds a thick electric-double layer near 0 V, delivering the highest capacitance (3000 → 1100 μF cm^{-2}) that drops steeply as the potential rises (PZC ≈ 0.25 V). And after adding Gly into the PAM gel electrolyte, it exhibits a denser framework and fewer

adsorption sites, so its capacitance is roughly halved (1500 → 700 μF cm^{-2}) while retaining the same potential dependence. Further introduction of zwitterions, it "locks" surface charges and confines ions within micropores, rendering the surface nearly charge-neutral; consequently, EDL thickness and ion adsorption become potential-independent, producing the lowest capacitance (<700 μF cm^{-2}) and a wide-voltage, zero-net-charge character. This invariant interfacial structure suppresses self-discharge and side reactions, enabling highly stable cycling (Fig. 4g) [41]. In theory, DAPS exhibited higher adsorption energy on Zn (101) plane compared to Zn (002) plane, promoting oriented deposition along the (002) plane, thereby synergistically enabling high interface stability and long-term cycling (Fig. 4h) [42].

Following closely, the Zn metal anode after cycling was analyzed to verify this fact. As shown in Fig. S10, compared to the pure PAM gel electrolyte system and the gel electrolyte only with Gly addition, Zn metal anode after cycling in the zwitterionic-functionalized gel electrolyte demonstrated a strong Zn (002) crystal plane, consistent with

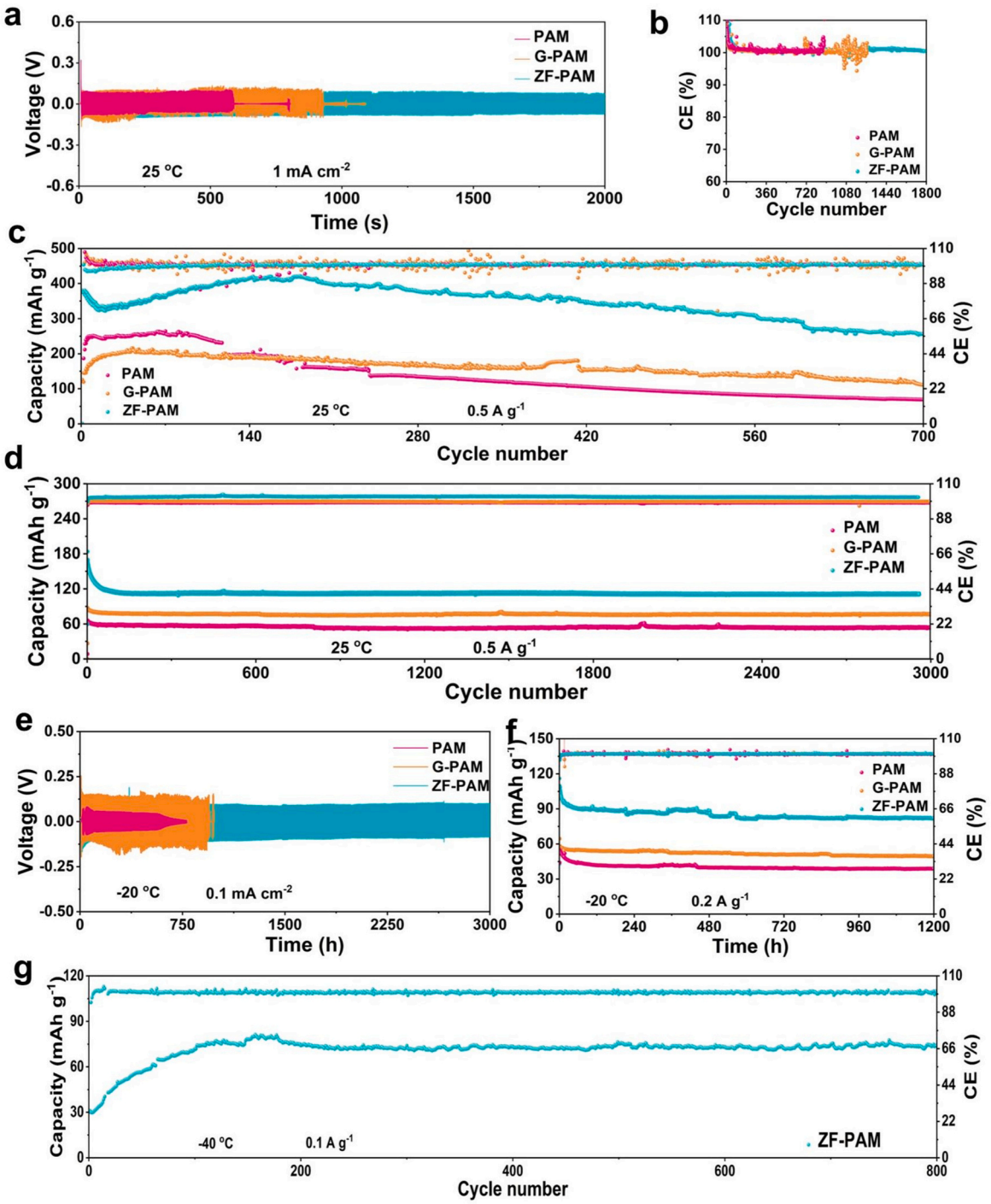

Fig. 5. Electrochemical performance and application. a) Long cycling stability of Zn || Zn symmetric cells at room temperature; b) long cycling stability of Cu | Zn half cells; c) cycling performance of NVO full cells at 0.5 A g^{-1}; d) cycling performance of Zn || I_2 cells at the current density of 0.5 A g^{-1} at room temperature; e) long cycling stability of Zn || Zn symmetric cells at −20 °C; f) cycling performance of Zn || I_2 cells at the current density of 0.2 A g^{-1} at −20 °C; g) cycling performance of Zn || PANI cells at the current density of 0.1 A g^{-1} at −40 °C.

theoretical analysis. Besides, the SEM images of Zn metal anode after cycling also demonstrated a smooth deposition morphology was observed when using the zwitterionic-functionalized gel electrolyte, while the Zn surface after cycling in the control group was uneven with many small protrusions and corrosion (Fig. 4i) [43]. To further visualize the homogeneity of the SEI layer, EDS mapping was performed on the cycled Zn anodes (Figs. S11–13). Furthermore, to assess the long-term interfacial stability beyond 50 cycles, SEM characterization was performed on zinc metal surfaces after 100 cycles. The ZF-PAM electrolyte still maintained a smooth and uniform surface, further confirming the sustained dendrite-suppressing capability and robust interfacial stability afforded by the zwitterionic functionalization over extended cycling (Fig. S14). Long-term cycling stability of Zn metal anode is further attributed to a robust SEI, which was analyzed by TEM and XPS. As shown in Fig. 4j & k, when cycling in the zwitterionic-functionalized gel electrolyte, a compact and clearly visible SEI layer with a thickness of ~11.2 nm can be observed on the Zn surface. High-resolution TEM images revealed distinct lattice fringes corresponding to ZnS, ZnF_2, and ZnO, confirming the formation of a ZnF_2-ZnS-rich interphase during long-term electrochemical cycling. This can be attributed to the ability of DAPS to immobilize anions from the Zn salt via its charged functional groups, which increased the Zn^{2+} transference number and promoted the formation of a uniform and robust SEI layer. This was also consistent with XPS results. As shown in Fig. 4l & m, the peaks at 162.0 eV and 684.8 eV can be attributed to ZnS and ZnF_2 components in the SEI film, respectively. And the intensified signals for ZnS and ZnF_2 in the zwitterionic-functionalized gel electrolyte systems confirmed the formation of compact and robust SEI layer. This stable SEI layer promoted highly reversible Zn plating/stripping and rapid Zn^{2+} kinetics at low temperature [44]. To further elucidate the spatial distribution of the SEI, XPS depth profiling (Ar^+ sputtering) was conducted. As presented in Fig. S15, the signal intensities of ZnF_2 (F 1s) and ZnS (S 2p) exhibit a gradual increase with etching depth, revealing an inorganic-rich gradient toward the inner interface. Ex-situ SEM of Zn anodes cycled at −20 °C and −40 °C further confirmed dendrite suppression. The PAM electrolyte showed large protrusions and cracks, whereas ZF-PAM maintained a flat surface (Fig. S16), highlighting its effectiveness under extreme cold.

2.4. Electrochemical performance and application

The Zn || Zn symmetric cells were first employed to explore the electrochemical performance of gel electrolytes. As shown in Fig. 5a, the symmetric cells using the zwitterionic-functionalized gel electrolyte achieved stable cycling for over 2000 h at the current density of 1.0 mA cm^{-2}, whereas reference gel electrolyte systems fail within 1000 h due to continuous interface side reactions and uncontrolled Zn dendrite growth. Similarly, Zn | Cu half cells were also assembled to evaluate the CE, which was shown in Fig. 5b. When using the pure PAM gel electrolyte, the half cells failed after ~1000 cycles due to severe Zn dendrite growth and unstable interface, while the CE in the zwitterionic-functionalized gel electrolyte system can maintain stable over 1800 cycles, indicating high reversibility, which can be attributed the robust SEI layer.

Then, this work assembled full cells with an NVO cathode and analyzed their self-discharge behavior. As shown in Fig. S17, after 24 h of open-circuit standing, the full cell using the zwitterionic-functionalized gel electrolyte retained 95 % of its initial capacity, significantly outperforming the pure PAM gel electrolyte and the gel electrolyte only with Gly addition, which retained only 85 ± 2 % and exhibited noticeable voltage decay. Furthermore, under the zwitterionic-functionalized gel electrolyte, full cells with NVO cathode can also display a more outstanding rate performance, especially at high current density, which can be attributed better Zn^{2+} kinetics (Fig. S18). For the cycling stability, the DAPS-based full cells delivered an initial discharge capacity of 395 mAh g^{-1} and maintained a high capacity retention of over 700 cycles (Fig. 5c), much higher than that in the pure PAM gel electrolyte and the gel electrolyte only with Gly addition, which further proved the advancement of zwitterionic-functionalized gel electrolyte in suppressing side reactions and energy dissipation. This work further extended the evaluation to a Zn—I_2 battery system. As shown in Fig. 5d, the full cells using the zwitterionic-functionalized gel electrolyte cycled stably for 3000 cycles with a high capacity of 120 mAh g^{-1} at the current density of 0.5 A g^{-1}, indirectly illustrating its high interface stability, but the capacity of full cells cycled in the pure PAM gel electrolyte was as low as <60 mAh g^{-1}.

Futthermore, to verify the practical application of the zwitterionic-functionalized gel electrolyte in low-temperature zinc-ion batteries, symmetric cells were first tested at −20 °C. As shown in Fig. 5e, the DAPS-modified electrolyte supported stable Zn plating/stripping for over 3000 h, far exceeding the pure PAM gel electrolyte. Even under a more challenging condition of −40 °C, the cell still maintained stable operation for 1500 h (Fig. S19), showing excellent application prospects. However, the pure PAM gel electrolyte froze at −40 °C, causing the battery to malfunction. And for full cells, a stable capacity of 90 mAh g^{-1} with prolonged cycling was observed when using the zwitterionic-functionalized gel electrolyte, while the full cells cycling in the pure PAM gel electrolyte showed a low discharge capacity and cycling life (Fig. 5f). Even at −40 °C, the full cells paired with polyaniline cathode can also provide a consistent discharge capacity around 70 mAh g^{-1} and continue operating over 800 cycles (Fig. 5g).

Based on the above results, the incorporation of DAPS facilitates the formation of a uniform and robust SEI layer, enabling integrated improvements in capacity, CE, and cycle life across a broad temperature range from −40 °C to room temperature, underscoring the considerable promise of zwitterion-functionalized electrolytes for practical low-temperature zinc-ion batteries.

3. Conclusion

In summary, this work have successfully developed a zwitterion-functionalized gel electrolyte capable of modulating hydrogen bonding networks and effectively confining free water molecules, thereby depressing the freezing point below −40 °C. The copolymerization of DAPS not only significantly improves the gel electrolyte toughness but widens the spacing between polymer chains, thereby constructing rapid and stable Zn^{2+} transport channel. Simultaneously, this electrolyte facilitates the in situ formation of a uniform, robust SEI film with a thickness of approximately 11.2 nm on the Zn anode surface. The zwitterion-functionalized gel electrolyte maintains high interfacial stability, regulates Zn^{2+} migration and deposition behavior, and promotes uniform zinc plating. As a result, it demonstrates excellent compatibility with various cathode materials including NVO, I_2, and PANI. Notably, Zn—I_2 full cells retain high capacity and stability over 3000 cycles at room temperature, and maintain remarkable performance even at −40 °C. This work provides a feasible and versatile molecular-scale design strategy for advanced gel electrolytes, significantly promoting the application prospects of AZIBs under low temperature.

4. Experimental section

Preparation of gel electrolytes. Firstly, we added 2.1 g of acrylic acid amide (AM) monomer, 0.9 g of Glycine (GIY), 0.8 g of 3-[(3-Acrylamidopropyl)dimethylammonio]propane-1-sulfonate (DAPS), 7.27 g of zinc trifluoromethanesulfonate ($Zn(OTf)_2$) to 10 mL of deionized water, and stirred thoroughly until all components were completely dissolved to form a clear solution. Next, we needed to prepare two solutions: one was a 3.0 g/L crosslinking agent *N*,*N*′-methylenebisacrylamide (MBA) solution, and the other was a 20 g/L initiator ammonium persulfate (APS) aqueous solution. The two solutions were added to the clarified solution in proportions, with 700 μL each of MBA and APS, and poured into the

mold after thorough mixing. After that, a polymerization reaction was carried out on a hot plate at 70 °C to form a quasi-solid gel, we prepared a pure gel electrolyte, which had the same preparation conditions, with the only difference being that GIY and DAPS was not added. This work also prepared a G-PAM gel electrolyte, which had the same preparation conditions, with the only difference being that DAPS was not added.

CRediT authorship contribution statement

Mengfan Zhao: Writing – review & editing, Writing – original draft, Validation, Methodology, Investigation, Formal analysis, Data curation, Conceptualization. **Xueqing Chen:** Data curation. **Shuai Liu:** Formal analysis. **Rujian Fu:** Formal analysis. **Bao Li:** Data curation. **Lifeng Hou:** Validation, Project administration. **Shi Wang:** Writing – review & editing, Investigation. **Zhong Jin:** Writing – original draft, Investigation. **Qian Wang:** Funding acquisition.

Declaration of competing interest

The authors declare that they have no known competing financial interests or personal relationships that could have appeared to influence the work reported in this paper.

Acknowledgements

This work was supported by the National Natural Science Foundation of China (No. 22402146), the Beijing Natural Science Foundation-Xiaomi Innovation Joint Foundation (L223011), Young Elite Scientists Sponsorship Program by CAST (2022QNRC001), Shanxi Energy Internet Research Institute (SXEI2023A004), Open Research Fund of Guangdong Advanced Carbon Materials Co., Ltd. (Kargen-2024B0905), the special fund for Science and Technology Innovation Teams of Shanxi Province (202204051001004), and the Open Fund of Key Laboratory of Functional Molecular Solids of Ministry of Education (FMS2025009).

Appendix A. Supplementary data

Supplementary data to this article can be found online at https://doi.org/10.1016/j.cej.2025.171875.

Data availability

Data will be made available on request.

References

[1] J. Zhang, M. Shi, H. Gao, X. Ren, J. Cao, G. Li, A. Wang, C. Liu, Engineering interfaces of zinc metal anode for stable batteries, Chem. Eng. J. 491 (2024) 152050, https://doi.org/10.1016/j.cej.2024.152050.
[2] N. Jiang, J. Zhu, C. Li, X. Liu, X. Guo, C. Zhu, Y. Chen, Y. Zhou, W. Deng, R. Li, Interfacial modulation of nicotinamide additive enables 9700 h Zn metal batteries, J. Colloid Interface Sci. 677 (2025) 645–654, https://doi.org/10.1016/j.jcis.2024.07.253.
[3] G. Wu, W. Yang, Y. Yang, Y.-K. Choe, E. Yoo, Zinc-ion conductive metal–organic framework interfaces for comprehensive anode protection in high-performance aqueous zinc-ion batteries, ACS Nano 19 (2025) 18244–18255, https://doi.org/10.1021/acsnano.4c18162.
[4] M. Zhang, H. Wei, Y. Zhou, W. Wen, L. Zhang, X.-Y. Yu, A multi-functional protective material with atomically dispersed zincophilic sites enabling long-life zinc anodes, Chem. Sci. 15 (2024) 18187–18195, https://doi.org/10.1039/D4SC04385E.
[5] Y. Hou, S. Liu, S. Wang, W. Zhang, S. Li, J. Qiu, Achieving uniform deposition of Zn with amide additives for metal anodes stabilization, ACS Appl. Mater. Interfaces 16 (2024) 67821–67829, https://doi.org/10.1021/acsami.4c16497.
[6] M. Zhang, H. Wei, Y. Zhou, W. Wen, L. Zhang, X.-Y. Yu, A multi-functional protective material with atomically dispersed zincophilic sites enabling long-life zinc anodes, Chem. Sci. 15 (2024) 18187–18195, https://doi.org/10.1039/D4SC04385E.
[7] K. Brinkert, P. Mandin, Fundamentals and future applications of electrochemical energy conversion in space, Npj Microgravity 8 (2022) 52, https://doi.org/10.1038/s41526-022-00242-3.
[8] T. Sun, S. Zheng, H. Du, Z. Tao, Synergistic effect of cation and anion for low-temperature aqueous zinc-ion battery, Nano Micro Lett. 13 (2021) 204, https://doi.org/10.1007/s40820-021-00733-0.
[9] G. Mao, P. Xu, X. Liu, X. Zhao, Z. Shen, D. Chao, M. Chen, Prioritized Na+ adsorption-driven cationic electrostatic repulsion enables highly reversible zinc anodes at low temperatures, Nano Micro Lett. 18 (2026) 47, https://doi.org/10.1007/s40820-025-01889-9.
[10] F. Grzegorzewski, A. Benhaim, Y. Itzhaik Alkotzer, E. Zelinger, N. Yaakov, G. Mechrez, In situ fabrication of multi-walled carbon nanotubes/silica hybrid colloidosomes by Pickering emulsion templating using trialkoxysilanes of opposite polarity, Polymers 11 (2019) 1480, https://doi.org/10.3390/polym11091480.
[11] M.Z. Ansari, S.N. Banitaba, S. Khademolqorani, I. Kamika, V.V. Jadhav, Overlooked promising green features of electrospun cellulose-based fibers in lithium-ion batteries, ACS Omega 8 (2023) 43388–43407, https://doi.org/10.1021/acsomega.3c05068.
[12] Y. Sheng, J. Yang, X. Zhao, H. Liu, S. Cui, L. Chen, R. Zeng, X. Wang, C.-H. Huang, W. Li, Development and *in vitro* biodegradation of biomimetic zwitterionic phosphorylcholine chitosan coating on Zn1Mg alloy, ACS Appl. Mater. Interfaces 12 (2020) 54445–54458, https://doi.org/10.1021/acsami.0c16662.
[13] Q. Wang, J. Huang, L. Qi, M. Li, S. Wang, J. Chen, Z. Sui, T. Bi, Q. Tang, L. Yu, P. Hu, W. Zhang, C. Lu, C. Chen, A bioinspired gradient hydrogel electrolyte network with optimized interfacial chemistry toward robust aqueous zinc-ion batteries, ACS Nano 19 (2025) 26770–26781, https://doi.org/10.1021/acsnano.5c06914.
[14] X. Yan, J. Zhang, Y. Sheng, K. Chen, H. Zhao, Q. Zhang, Y. Cheng, Z. Ge, X. Ming, Y. Zhang, Decoupling the trade-off between mechanical properties and ionic conductivity in hydrogel polymer electrolytes by anomalous water-induced microphase separation, ACS Nano (2025) acsnano.5c16323, https://doi.org/10.1021/acsnano.5c16323.
[15] L. Wang, H. Wang, J. Cao, J. Yan, C. Dai, W. Sun, Q. Du, Z. Huang, D. Liu, C. Li, J. Sun, Restructuring hydrogen bond networks in polyacrylamide hydrogels via trehalose additives for wide-temperature-range Zn-ion batteries, ACS Nano 19 (2025) 28397–28409, https://doi.org/10.1021/acsnano.5c06805.
[16] V.P. Nguyen, M. Park, Y.-W. Byeon, S. Lim, K. Yim, M. Oh, S. Hyun, E. Jeon, S.-M. Lee, Ultrathin yet effective: 90 nm ZnF_2 layer for stabilizing zinc–metal anodes, ACS Energy Lett. 10 (2025) 5503–5511, https://doi.org/10.1021/acsenergylett.5c02565.
[17] Y. Yuan, J. Chen, T. Qian, B. Zhang, K. Ye, R. Li, X. Yang, Hydrogen atom capture toward dense solid electrolyte interface for long-cycling aqueous zinc-ion batteries, Angew. Chem. Int. Ed. 64 (2025) e202513722, https://doi.org/10.1002/anie.202513722.
[18] C. Chang, S. Hu, T. Li, F. Zeng, D. Wang, S. Guo, M. Xu, G. Liang, Y. Tang, H. Li, C. Han, H.-M. Cheng, A robust gradient solid electrolyte interphase enables fast Zn dissolution and deposition dynamics, Energy Environ. Sci. 17 (2024) 680–694, https://doi.org/10.1039/D3EE03422D.
[19] B. Guo, J. Jia, Y. Zhao, J. Zhang, G. Li, K. Chen, A. Wang, C. Liu, Innovative zwitterionic polymers in advanced batteries, Energy Storage Mater. 78 (2025) 104253, https://doi.org/10.1016/j.ensm.2025.104253.
[20] Q. Yang, W. Yang, Z. Wang, R. Chen, M. Li, C. Qin, D. Gao, W. Chen, Strong and tough antifreezing hydrogel sensor via the synergy of coordination and hydrogen bonds, ACS Appl. Mater. Interfaces 15 (2023) 51684–51693, https://doi.org/10.1021/acsami.3c10205.
[21] C.-F. Xiao, Y.-X. Lu, M. Lu, D. Luo, K. Xiao, Y. Wang, Z.-Q. Liu, A dynamic amphiphilic additive with dual solubility modulates Zn^{2+} solvation and *in situ* SEI for a dendrite-free zinc anode, Chem. Sci. 16 (2025) 13655–13666, https://doi.org/10.1039/D5SC03646A.
[22] J. Ba, X. Li, J. Li, X. Yin, Y. Wei, Y. Ding, K. Zhao, Y. Wang, Sustained release of underpotential deposition initiators for ah-level zinc metal batteries, Angew. Chem. Int. Ed. (2025) e202514181, https://doi.org/10.1002/anie.202514181.
[23] Q. Wan, B.C. Thompson, Control of properties through hydrogen bonding interactions in conjugated polymers, Adv. Sci. 11 (2024) 2305356, https://doi.org/10.1002/advs.202305356.
[24] Y. Liao, H. Zheng, L. Dai, F. Li, G. Zhu, Q. Guan, Y. Sun, X. Tang, Hydrophobically modified polyacrylamide synthesis and application in water treatment, Asian J. Chem. 26 (2014) 5923–5927, https://doi.org/10.14233/ajchem.2014.16860.
[25] H. Zheng, H. Zhou, B. Zheng, C. Wei, A. Ma, X. Jin, W. Chen, H. Liu, Stable flexible electronic devices under harsh conditions enabled by double-network hydrogels containing binary cations, ACS Appl. Mater. Interfaces 16 (2024) 7768–7779, https://doi.org/10.1021/acsami.3c17057.
[26] M. Zhao, B. Zhang, X. Bai, J. Zhang, X. Chang, L. Hou, H. Huang, S. Wang, Z. Jin, Q. Wang, Competitive Li+ coordination in gel electrolyte enhances Zn2+ kinetics and interfacial stability for low-temperature Zn-ion batteries, Chem. Eng. J. 520 (2025) 166042, https://doi.org/10.1016/j.cej.2025.166042.
[27] X. Chen, C. Liu, X. Bai, J. Zhang, X. Chang, L. Hou, H. Huang, Y. Wei, B. Wu, W. Liu, Q. Wang, A thin and homogeneous solid electrolyte interface enriched with ZnF2 and ZnS for highly reversible zinc batteries, Energy Storage Mater. 75 (2025) 103984, https://doi.org/10.1016/j.ensm.2024.103984.
[28] D. Lin, Y. Lin, R. Pan, J. Li, A. Zhu, T. Zhang, K. Liu, D. Feng, K. Liu, Y. Zhou, C. Yang, G. Hong, W. Zhang, Water-restrained hydrogel electrolytes with repulsion-driven cationic express pathways for durable zinc-ion batteries, Nano Micro Lett. 17 (2025) 193, https://doi.org/10.1007/s40820-025-01704-5.
[29] T. Lu, Y. Lin, L. Guan, L. Hou, H. Du, H. Wei, X. Liu, C. Yang, Y. Wei, M. Song, W. Liu, H. Zhou, Q. Wang, Suppressing side reaction and dendritic growth via interfacial cyclization molecule for stable Zn metal anodes, ACS Appl. Energy Mater. 7 (2024) 61–71, https://doi.org/10.1021/acsaem.3c02209.

[30] Y. Xiong, H. Cheng, Y. Jiang, Z. Fan, X. Li, G. Wang, T. Liu, X. Gu, A novel water-reducer-based hydrogel electrolyte for robust and flexible Zn-I2 battery, Energy Storage Mater. 74 (2025) 103981, https://doi.org/10.1016/j.ensm.2024.103981.
[31] Z. Wang, G. Sun, N.H.C. Lewis, M. Mandal, A. Sharma, M. Kim, J.M. Montes De Oca, K. Wang, A. Taggart, A.B. Martinson, P.A. Kohl, A. Tokmakoff, S.N. Patel, P. F. Nealey, J.J. De Pablo, Water-mediated ion transport in an anion exchange membrane, Nat. Commun. 16 (2025) 1099, https://doi.org/10.1038/s41467-024-55621-z.
[32] R. Fu, B. Zhang, T. Lu, C. Liu, L. Hou, S. Wang, Y. Ning, Z. Jin, Q. Wang, A dilute and non-flammable electrolyte engineering enables stable SEI for low-temperature zinc batteries, Energy Storage Mater. 80 (2025) 104374, https://doi.org/10.1016/j.ensm.2025.104374.
[33] X. Liang, X. Chen, Z. Zhai, T. Yu, H. Yu, H. Wang, D. Meng, L. Peng, S. Yin, Synergistic modulation of hydrogen bond network reconstruction and pH buffering of electrolyte enables highly reversible Zn anode, Chem. Eng. J. 493 (2024) 152622, https://doi.org/10.1016/j.cej.2024.152622.
[34] Z. Yao, T. Fu, T. Pan, C. Luo, M. Pang, S. Xiong, Q. Guo, Y. Li, S. Liu, C. Zheng, W. Sun, Dynamic doping and interphase stabilization for cobalt-free and high-voltage lithium metal batteries, Nat. Commun. 16 (2025) 2791, https://doi.org/10.1038/s41467-025-58110-z.
[35] Q. Wang, B. Xu, Y. Du, L. Kuang, Z. Lin, X. Gu, A cost-effective pyrrole additive for realizing highly stable Zn anode, Rare Metals 44 (2025) 209–217, https://doi.org/10.1007/s12598-024-02927-y.
[36] Q. Zheng, L. Liu, Z. Hu, Z. Tang, H. Lu, Y. Gao, J. Wang, Y. Song, C. Han, W. Li, Altering the Zn^{2+} migration mechanism enables the composite hydrogel electrolytes with high Zn^{2+} conduction and superior anti-dehydration, Adv. Funct. Mater. 35 (2025) 2504782, https://doi.org/10.1002/adfm.202504782.
[37] M. Shi, J. Zhang, G. Tang, B. Wang, S. Wang, X. Ren, G. Li, W. Chen, C. Liu, C. Shen, Polyzwitterionic cross-linked double network hydrogel electrolyte enabling high-stable Zn anode, Nano Res. 17 (2024) 5278–5287, https://doi.org/10.1007/s12274-024-6525-5.
[38] B. Li, B. Zhang, X. Bai, J. Zhang, X. Chang, L. Hou, H. Huang, T. Lu, S. Wang, Z. Jin, Q. Wang, A dynamic self-healing protective layer enabling stable zinc ion batteries through strong Zn-S affinity and intramolecular hydrogen bonding, Angew. Chem. Int. Ed. 64 (2025) e202503345, https://doi.org/10.1002/anie.202503345.
[39] S. Liu, B. Wu, X. Bai, J. Zhang, X. Chang, L. Hou, H. Huang, Y. Wei, S. Wang, Z. Jin, Q. Wang, A solvent-induced solid polymer electrolyte with controllable polymerization for low-temperature lithium metal batteries, Nano Lett. 25 (2025) 5241–5249, https://doi.org/10.1021/acs.nanolett.4c06471.
[40] D. Ma, F. Li, K. Ouyang, Q. Chen, J. Zhao, M. Chen, M. Yang, Y. Wang, J. Chen, H. Mi, C. He, P. Zhang, An electrochemically driven hybrid interphase enabling stable versatile zinc metal electrodes for aqueous zinc batteries, Nat. Commun. 16 (2025) 4817, https://doi.org/10.1038/s41467-025-60190-w.
[41] L. Jiang, D. Li, X. Xie, D. Ji, L. Li, L. Li, Z. He, B. Lu, S. Liang, J. Zhou, Electric double layer design for Zn-based batteries, Energy Storage Mater. 62 (2023) 102932, https://doi.org/10.1016/j.ensm.2023.102932.
[42] R. Deng, Z. He, F. Chu, J. Lei, Y. Cheng, Y. Zhou, F. Wu, An aqueous electrolyte densified by perovskite SrTiO3 enabling high-voltage zinc-ion batteries, Nat. Commun. 14 (2023) 4981, https://doi.org/10.1038/s41467-023-40462-z.
[43] L. Kuang, B. Xu, L. Zhang, Z. Lin, X. Gu, X. Ren, Y. Hou, Zincophilic and hydrophobic bifunctional PFA-COOH-CNT artificial SEI film for highly stable Zn anode, Nano Res. 18 (2025) 94907156, https://doi.org/10.26599/NR.2025.94907156.
[44] J. Ge, Y. Zhang, Z. Xie, H. Xie, W. Chen, B. Lu, Tailored ZnF2/ZnS-rich interphase for reversible aqueous Zn batteries, Nano Res. 16 (2023) 4996–5005, https://doi.org/10.1007/s12274-022-5325-z.